Journal of Power Sources 250 (2014) 181–187

Contents lists available at ScienceDirect

Journal of Power Sources

journal homepage: www.elsevier.com/locate/jpowsour

Single crystalline VO_2 nanosheets: A cathode material for sodium-ion batteries with high rate cycling performance

Wei Wang [a], Bo Jiang [a], Liwen Hu [a], Zheshuai Lin [b], Jungang Hou [a], Shuqiang Jiao [a,*]

[a] State Key Laboratory of Advanced Metallurgy, University of Science and Technology Beijing, No. 30 Xueyuan Road, Beijing 100083, PR China
[b] Technical Institute of Physics and Chemistry, Chinese Academy of Sciences, Beijing 100190, PR China

HIGHLIGHTS

- The single crystalline VO_2 nanosheets have been synthesized.
- The reaction during charge/discharge can happen between $Na_{0.3}VO_2$ and $NaVO_2$.
- The synthesized material can retain outstanding rate ability.

ARTICLE INFO

Article history:
Received 18 June 2013
Received in revised form
21 October 2013
Accepted 10 November 2013
Available online 19 November 2013

Keywords:
Sodium-ion batteries
Vanadium oxides
Nanosheet
Cathode materials

ABSTRACT

In recent years, with the growing demands for large-scale applications of rechargeable batteries, the eco-friendly sodium-ion batteries with low price and high charge–discharge rates have attracted much attention. In this work, using a simple hydrothermal process, we successfully synthesize single crystalline VO_2 parallel ultrathin nanosheets for the cathode material in sodium-ion batteries. Combined the XRD, XPS, electrochemical measurements with the first-principles simulations, the charge–discharge performance and the mechanism of Na insertion and extraction into/from the VO_2 structure have systematically studied. The results reveal that the Na_xVO_2 products possess semiconductor properties and the interlayer distance almost keeps constant during charge and discharge process, which is beneficial to the transmission of Na ions. The charge and discharge process occurs between $Na_{0.3}VO_2$ and $NaVO_2$. Even at a large current density of 500 mA g^{-1}, the discharge capacity can still keep at 108 mAh g^{-1}. As a cathode material for sodium-ion batteries, the results are outstanding and provide a possibility of large-scale applications for rechargeable sodium-ion batteries.

1. Introduction

Lithium ion batteries with high energy and power densities have been considered as the best power sources for portable equipment today [1–4]. However, there is a serious concern about the availability of lithium for the limit of lithium reserves in the earth, especially in large-scale applications [5–8]. On this occasion, the eco-friendly sodium-ion batteries have become the focus in the field of energy and environment for the abundance of sodium [9–12]. Recently, a number of cathode materials have been extensively investigated as potential electrode materials for sodium-ion batteries, such as $NaNi_{1/3}Mn_{1/3}Co_{1/3}O_2$ [13], $Na_{0.44}MnO_2$ [14], $NaFePO_4$ [15], $NaMnFe_2(PO4)_3$ [16], V_2O_5 [17], $Na_3V_2(PO_4)_3$ [18], $Na_2V_6O_{16}$ [19], $NaFeF_3$ [20], $NiCo_2O_4$ [21]. Nevertheless, few of the reported cathode materials are qualified for battery applications for either their low storage capacity or poor cycling ability.

Vanadium oxides have attracted great attention for their outstanding structural flexibility combined with interesting chemical and physical properties, and they have been widely used in catalysts [22], chemical sensors [23], electrochemical and optical devices [24] and lithium ion batteries [25,26]. Of the various known vanadium oxides, metastable vanadium dioxide VO_2 (B) is of great interest owing to its layered structure and promising properties in the nanometer domain [27–29]. The structure of VO_2 (B) are built-up distorted VO_6 octahedra, which shares both corners and edges [30,31], forming the V–O tunnels perpendicular to the *c*-axis.

Nanostructured VO_2 (B) has been prepared and studied as a cathode material of lithium-ion batteries for years [25,26,32]. However, to the best of our knowledge, its application in sodium-ion batteries has not been reported. In this paper, metastable monoclinic VO_2 (B) parallel ultrathin nanosheets have been successfully synthesized. Due to the phase change from metastable

* Corresponding author. Tel./fax: +86 10 62334204.
E-mail address: sjiao@ustb.edu.cn (S. Jiao).

0378-7753/$ – see front matter © 2013 Elsevier B.V. All rights reserved.
http://dx.doi.org/10.1016/j.jpowsour.2013.11.016

VO_2 (B) to thermodynamically more stable rutile VO_2 at $T > 300$ °C [33], the synthetic experiments were performed through a low temperature hydrothermal method. The synthesized material is semiconducting metal oxide with a low-dimension, and owing to its single-crystalline structure and high surface-to-volume ratio, the rate and cycling performance is excellent among varieties of cathode materials for sodium-ion batteries.

2. Experimental and theoretical methods

All chemicals were analytical grade and used without further purification. The single crystalline VO_2 nanosheets were synthesized within a very short time through a hydrothermal method. Firstly, 30 mL ethylene glycol and 45 mL distilled water were mixed together in a 150 mL beaker, and then 2.5 g V_2O_5 was added to the beaker. The above solution was pretreated for 30 min under ultrasonic vibration condition till a uniform yellow suspension was formed. The aqueous solution was transferred to a sealed Teflon-lined stainless steel autoclave and heated at 160 °C for 3 h. Subsequently, the autoclave was quenched in a cold bath. A dark green precipitate was formed and collected with distilled water and ethanol by a centrifuge, and then dried in an oven at 120 °C overnight.

The morphology of VO_2 powders was characterized by transmission electron microscopy (TEM, JEOL, JEM-2010). The crystal structure of VO_2 powders was characterized by X-ray diffraction measurement (XRD, Rigaku, D/max-RB) using Cu Kα radiation in a 2θ range from 10° to 90° at room temperature.

Positive electrodes were fabricated by mixing 75 wt % of active material VO_2, 15 wt % of acetylene black and 10 wt % of teflon (poly(tetrafluoroethylene), PTFE) binder, and then coated uniformly on an aluminum foil. Finally, the electrode was dried at 120 °C for 12 h. The electrolyte used was a 1.0 M $NaClO_4$ in a propylene carbonate (PC) electrolyte solution. A glass fiber (GF/D) from Whatman was used as the separator. Coin cells were assembled in an argon filled glovebox. The active material electrode was used as the working electrode, and Na foil was used for both counter and reference electrodes. Galvanostatic charge and discharge cycles were conducted at room temperature under different current densities with a voltage between 1.5 and 4.0 V. X-ray photoelectron spectroscopy (XPS, Kratos AXIS Ultra DLD) was applied to analyze the valent state of vanadium after a charge/discharge process. The coin cell was also measured by electrochemical impedance spectroscopy (EIS, Solatron 1287/1255B) to evaluate the electrochemical performance, redox processes and the ionic and electronic conductivity with a frequency range from 100 kHz to 0.1 Hz.

To illustrate the insertion–extraction mechanism of sodium ions in the VO_2 electrode, the first-principles plane-wave pseudopotential method [34] implemented in the CASTEP package [35] were employed to calculate the formation energy and unit cell volume change for Na-ion insertion. Generalized gradient approximation with norm-conserving pseudopotentials [36] was used with the plane-wave cut-off of 400 eV. In order to study Na insertion and extraction, it is necessary to consider a larger cell than the basic unit. Thus we construct a supercell of four unit ($2 \times 2 \times 1$) cells consisting of 8 Na_xVO_2 molecules. Brillouine-zone integrations are made using ($2 \times 3 \times 4$) special-*k*-point meshes according to the Monkhorst-Pack scheme [37]. For each geometry optimization both atomic positions and lattice parameters are fully relaxed using the quasi-Newton method [38]. The convergence thresholds between optimization cycles for energy change, maximum force, maximum stress, and maximum displacement are set as 2×10^{-5} eV/atom, 0.05 eV Å^{-1}, 0.1 GPa, and 0.002 Å, respectively. The optimization terminates when all of these criteria are satisfied. The choice of these computational parameters ensures good convergence in present studies.

As sodium ions are successively incorporated into the V–O (VO) tunnel, the formation energy is defined as:

$$E_f(\mathrm{Na}) = [E_{tot}(n\mathrm{Na} + \mathrm{VO}) - E_{tot}(\mathrm{VO}) - n \cdot E_{tot}(\mathrm{Na})]/n \quad (1)$$

Here $E_{tot}(n\mathrm{Na} + \mathrm{VO})$ is the total energy of the VO tunnel containing n sodium atoms in a unit cell, $E_{tot}(\mathrm{VO})$ is the total energy of the VO tunnel without any sodium atom, and $E_{tot}(\mathrm{Na})$ is the total energy of a sodium atom in the reservoir (i.e., bulk Na).

3. Results and discussion

The TEM and HRTEM images of the VO_2 powders are shown in Fig. 1(a) and (b). Overall, VO_2 is composed of numerous parallel ultrathin nanosheets. The nanosheets have an average diameter of ca. 50–60 nm and an average length of hundreds of nanometers, tending to assemble to form bundles of VO_2. These nanosheets are rapidly formed at a low temperature within a short time, which is much more efficient than other literature methods [39–43]. The HRTEM image of the tip of the nanosheet in Fig. 1(b) evidences the single crystalline nature of the nanosheets. The distance between the adjacent lattice fringes is 0.352 nm, which can be assigned to the interplanar distance of VO_2 nanostructures (110). This in combination with the selected-area electron diffraction (SAED) pattern (Fig. 1(c)) taken on a single nanosheet suggests the growth direction (110) of the nanosheet units and the single-crystalline nature, according to the Bragg equation. And this also corresponds to Fig. 1(d). XRD pattern of the as-prepared VO_2 is shown in Fig. 1(d). The weak intensity and broad width of the XRD peaks are mainly attributed to the tiny size of the phase that results in the smearing of the measured signal strength.

To clear the theoretical capacity of VO_2 as a cathode material for sodium-ion batteries, the plane-wave pseudopotential method [34] implemented in the CASTEP package [35] was employed to investigate the insertion of sodium into the VO_2 structure.

The sheet-like structural feature of VO_2 implies that the sodium cations would be likely to insert into the VO_2 tunnels. Fig. 2(a) shows the calculated formation energy with respect to the number of sodium ions in a VO_2 molecule. As the number of the inserted Na ions increases from 0 to 1.0, the formation energy becomes more negative, indicating the formation of the more stable phase. Therefore, the Na-inserted process (discharge process) can happen spontaneously from the VO_2 to $NaVO_2$ phases. However, as the content x of Na ions excess 1.0, the formation energy of Na_xVO_2 (e.g. $Na_{1.125}VO_2$) becomes more positive compared with $NaVO_2$, which indicates that the latter is more stable, and on this occasion, the discharge process cannot take place spontaneously. Although the formation energy of $Na_{1.25}VO_2$ once again turns to a lower level, actually the V–O tunnels have been broken (see Fig. 2(b)).

Consequently, we suppose that about one Na ion in total might be located in a VO_2 molecule stably, and the result demonstrates that during Na intercalating and deintercalating process the reaction (2) might happen.

$$VO_2 + Na^+ + e = NaVO_2 \quad (2)$$

On the basis of reaction (2), the theoretical capacity of VO_2 is estimated to be 323 mAh g^{-1}.

Fig. 2(b) shows the volume change per VO_2 molecule during the Na ions inserting into the V–O lattice calculated from the first-principles theory. As the number of the located Na ions in a molecule ranges from 0.25 to 1.0, the volume change of Na_xVO_2 ($0.25 \leq x \leq 1.0$) is very little. The Na_xVO_2 compounds have almost the same structure as the original VO_2 nanosheet, except that Na ions are located in the interlayer space, as shown in the insert of Fig. 2(b). The detailed geometry analysis reveals that as the number

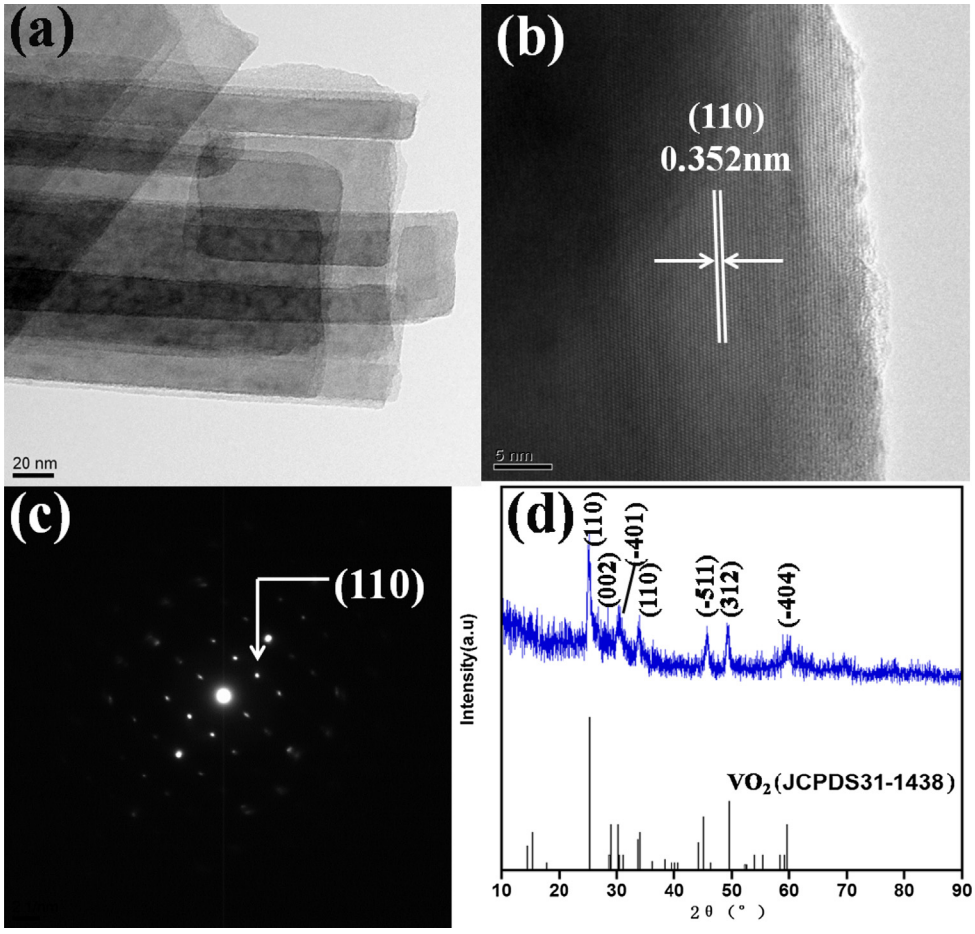

Fig. 1. TEM (a) and HRTEM (b) images of VO_2 nanosheets. (c) The corresponding SEAD pattern of VO_2 nanosheets. (d) X-ray diffraction patterns of the VO_2 nanosheets synthesized by hydrothermal.

of inserted Na ions per formula increases from 0.25 to 1, the interlayer distance changes from 5.96 Å to 5.56 Å and the decrease is only about 7% (see Fig. S1 and Table S1 in the Supporting information). The stable tunnel structure for the sodium transmission guarantees the intercalation and deintercalation of Na ions in a much easy and rapid manner. This makes it possible to charge and discharge at very high rates with less capacity decay in a Na ion battery as $x < 1.0$. For more Na ions inserted into the tunnels, the cell volume begins to expand consecutively. As $Na_{1.125}VO_2$ is formed, the cell volume is enlarged about 50% compared to that of a

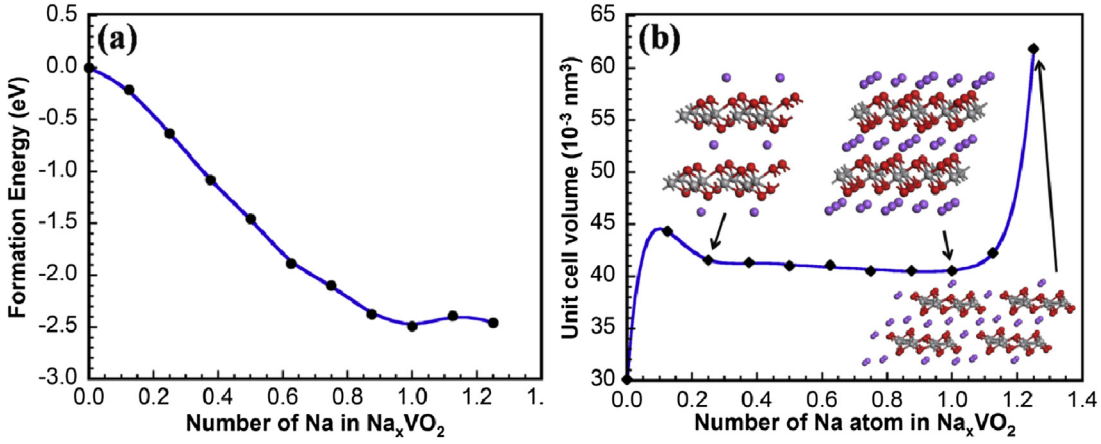

Fig. 2. (a) The relationship between the formation energy and the number of Na in Na_xVO_2. The blue curve is the exponential fitting for the calculated results. (b) Volume with respect to the number of Na ions in a VO_2 molecule. The insets illustrate the relaxed atomic structures with 0.25 Na, 1 Na and 1.25 Na, respectively, per VO_2 molecule. The purple spheres are Na atoms, the red spheres are oxygen atoms and the gray spheres are vanadium atoms. (For interpretation of the references to color in this figure legend, the reader is referred to the web version of this article.)

$NaVO_2$ unit cell. In this case, the distance between V and O is elongated to be 4.73 Å, which is much larger than the normal V–O chemical bond length (~2.3 Å). Thus, the backbone of the V–O tunnels are completely broken down (see insert of Fig. 2(b)), and the stability and reversibility of the VO_2-like structure is destroyed, so the charge–discharge processes cannot be fulfilled any more.

The electronic conductivity of Na_xVO_2 is evaluated by the band gap calculated by the first-principles method with respect to the number of sodium ions in a VO_2 molecule. Since the localized unclosed *d* shell in V cannot be correctly described by the Generalized Gradient Approximation (GGA) method, the GGA + *U* correction ($U = 3.1$ eV from the previous literature value [44]) is adopted to calculated the electronic band structures of Na_xVO_2. The very good agreement between the calculated and experimental band gaps (0.68 eV *vs.* 0.7 eV [44] for VO_2) demonstrate the validity of the first-principles calculations (see Fig. S2 and Table S2 in the Supporting information). The calculated results show that all band gaps in Na_xVO_2 ($0 < x < 1.0$) are less than 3 eV. This semiconductivity is helpful to the electrochemical properties due to its less resistance. In future, less carbon conductive additive may be used to increase the effective mass fraction.

The initial three charge and discharge curves of VO_2 (B) at the current density of 50 mA g^{-1} are illustrated in Fig. 3(a). The cut-off voltage was set in the range of 1.5–4.0 V *vs.* Na^+/Na. Before the regular galvanostatic charge/discharge tests, the cells were cycled at a relatively low current density for a period of time to fulfill the activation process. The initial discharge capacity is very high, as much as 214 mAh g^{-1}, while the charge and discharge capacities of the next two cycles change far less than the first two cycles. This can be attributed to the large surface area of the nanosheets, where some sodium ions are absorbed and contributed to the irreversible capacity in the initial cycle.

The fresh cell was measured by electrochemical impedance spectroscopy (EIS) at different bias voltages with a frequency range from 100 kHz to 0.1 Hz, and the corresponding Nyquist plots of the spectra were presented (Fig. 3(b)). Each impedance spectrum consists of a depressed semicircle at the high frequency followed by a slope line at the low frequency range. The depressed semicircle is attributed to charge-transfer impedance, while the slope line (about 45°) is due to Warburg impedance, attributable to the semiinfinite diffusion of sodium ions into the electrode–electrolyte interface [45,46]. In the EIS test, when different bias voltages are applied between anode and cathode electrodes, the charge transfer is significantly influenced. If the insertion and extraction of Na ions are not fast enough, the electrochemical impedance will rapidly increase under high bias voltages. As can be seen in Fig. 3(b), at different bias voltages from 2 to 4 V, no significant differences can be found in the Nyquist plots of the spectra, demonstrating a fast rate of insertion and extraction of Na ions. These results are due to the enlarged contact area of the nanosheets, which can provide shorter diffusion distance [47,48].

The V 2p XPS peaks of as-prepared VO_2 and Na_xVO_2 were analyzed to examine the valent state of the Na_xVO_2 surface before and after a discharge process in the second cycle at a low current density of 20 mA g^{-1}. Fig. 4(a) shows that only V^{4+} ions exist in the original powder, demonstrating that the as-prepared powder is VO_2, which is consistent with the XRD results. As shown in Fig. 4(b), almost only V^{3+} ions exist after a discharge process [49], which indicates that in this voltage range, about one Na ion is located in a VO_2 molecule, and at the end of discharging process, $NaVO_2$ is formed. The slight inconformity between the primitive curve and the fitting curve is due to a thimbleful of V^{4+}.

The V 2p XPS peaks after a charge process are also shown in Fig. 4(c). Both V^{3+} and V^{4+} ions can be clearly seen [49,50], and the amount of V^{4+} ions is much larger than V^{3+} ions, indicating that $NaVO_2$ is changed to Na_xVO_2 ($0 < x < 0.5$). The XPS results agree with the first-principles simulations shown in Fig. 2.

Fig. 5(a) shows the cyclability of the VO_2 electrode at different current densities from 10 mA g^{-1} to 500 mA g^{-1}. The results show that the specific discharge capacity gradually decreases with the increase of the charge/discharge current densities. When discharging at 20 mA g^{-1}, the specific discharge capacity can retain a reversible capacity of 179 mAh g^{-1} over 50 cycles, corresponding to a capacity retention ratio of 83.4% of the 10th cycle. Even at a very high current density of 500 mA g^{-1}, the capacity still remains 108 mAh g^{-1} over 50 cycles.

The capacity loss mainly occurs in the first few cycles, and two main reasons may be responsible for this phenomenon. (1) The small sized nanosheets have a large surface area, and some sodium ions are inserted in the surface of the nanotubes, which can contribute to the discharge capacity as the irreversible part, especially in the initial cycle [17]. (2) As the Na ions insert and extract into/from the Na_xVO_2 nanosheets, the volume adjustment occurs in the initial or second cycle, which may cause the capacity decay [9]. As a whole, the excellent performance is mainly due to the layered structure of Na_xVO_2 as well as the single crystalline and high specific surface area of the nanosheets. This layered structure can make the intercalation and deintercalation of Na ions much faster and

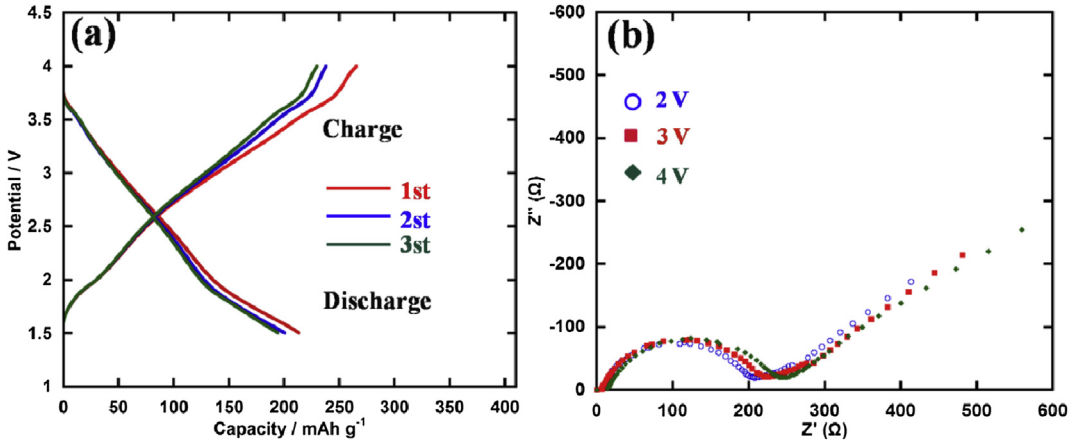

Fig. 3. The initial three charge and discharge curves of VO_2 at a current density of 50 mA g^{-1} between 1.5 and 4.0 V (*vs.* Na^+/Na). The electrochemical impedance spectroscopy of the as-prepared cells at different bias voltages.

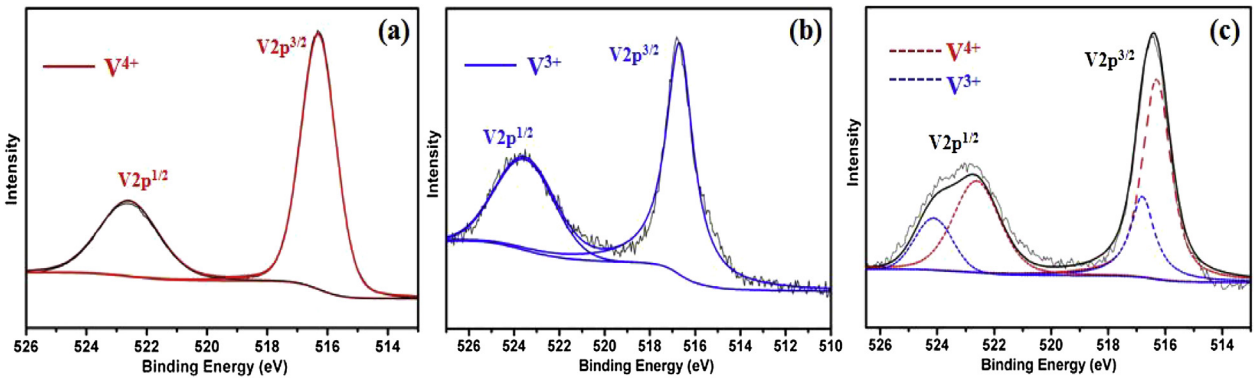

Fig. 4. XPS V 2p spectra of (a) VO_2 and (b) Na_xVO_2 after a discharge process and (c) after a charge process.

easier. The single crystalline was long-range ordered, crystal defect-free with a maintained, stable structure and improved capacity and cycle performance.

The nanosheet morphology is difficult to expand, and can also significantly increases the contact area between the active material and the liquid electrolyte, maintaining the original volume and realizing a high charge and discharge rate [51–55]. Indeed, as a battery material with such small size, the ionic and electronic diffusion distance is reduced and the penetration of sodium ions and electrons into the VO_2 nanosheets is much easier, thereby increasing the charge and discharge rate [52].

Generally, the first charge and discharge cycles are critical to represent the electrochemical performance for their complex mechanism. Here, the discharge capacity of the second and third cycle at a low current density is taken into account to evaluate the number of the inserted Na ions. When discharging at 20 mA g^{-1}, the discharge capacity of the second and third cycle is 235 mAh g^{-1} and 233 mAh g^{-1}, respectively, which indicates that ca. 0.7 Na ion is inserted in one VO_2 molecule. Therefore, on the basis of Figs. 2 and 4, the charge and discharge process occurs between $Na_{0.3}VO_2$ and $NaVO_2$.

An interesting result is that, at 10 mA g^{-1}, the capacity decays much faster than that of other current densities. This can be explained that, when charging at a relatively low current density, the full reduction of Na_xVO_2 to 1.5 V induces that it is difficult to complete extraction of Na ions at consequent charge process. Another reason is that, at such a low current density, the charge and discharge depth is more extensive, which may bring about a collapse of the crystallographic structure of this material [56].

To evaluate the rate performance and reversibility, the electrode was initially discharged at 1000 mA g^{-1} for 50 cycles and then at 20 mA g^{-1} for 20 cycles, as shown in Fig. 5(b). At such a high current density of 1000 mA g^{-1}, the discharge capacity can retain a reversible capacity of 70 mAh g^{-1} over 50 cycles, and the capacity retention from the initial to the last cycle is excellent. When the current density falls to 20 mA g^{-1}, the discharge capacity rises to 179 mAh g^{-1}, demonstrating an excellent reversibility and structural stability, even at very high Na-ion insertion and extraction velocities.

Fig. 6 shows the discharge behavior of the VO_2 battery at different current densities. In order to study the stability of the battery, it was kept working at every current density for decades of cycles. Fig. 6(a) depicts the performance of this battery from high current density to low current density, that is from 500 mA g^{-1} to 50 mA g^{-1}. For comparison purposes, Fig. 6(b) shows the performance of this battery at different current densities in reverse orders. As shown in Fig. 6(a), the electrode was initially discharged at 500 mA g^{-1} for 100 cycles and then at 200 mA g^{-1} for 50 cycles, at 100 mA g^{-1} for 50 cycles, and at 50 mA g^{-1} for 50 cycles, and the capacity is still maintain at 91 mAh g^{-1} after all these 250 cycles. This material displays an excellent cyclicity and reversibility. Nevertheless, when discharging from low to high current density, its performance suddenly becomes poor. The reason for this phenomenon is similar to that

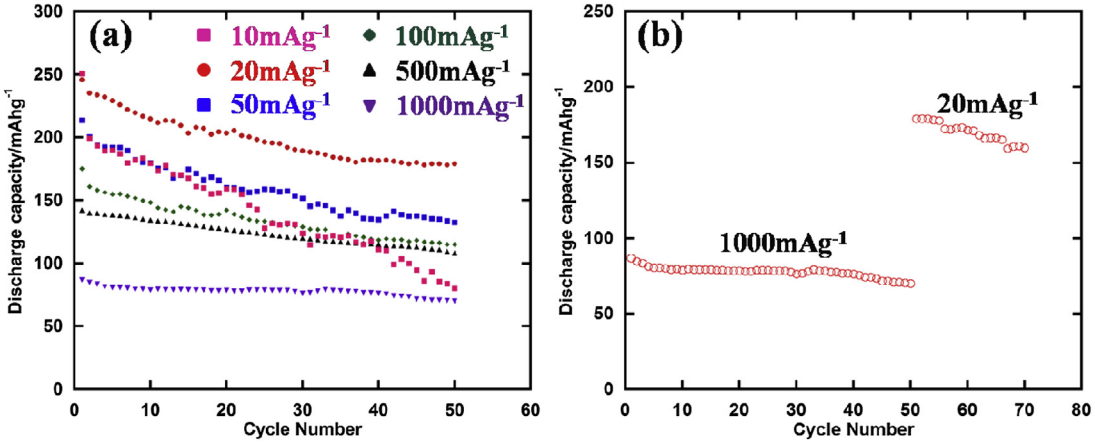

Fig. 5. (a) Discharge behavior of VO_2 battery at different current densities from 10 mA g^{-1} to 1000 mA g^{-1} over 50 cycles. (b) Rate capability plot showing cycling performance first at 1000 mA g^{-1} and next at 20 mA g^{-1}.

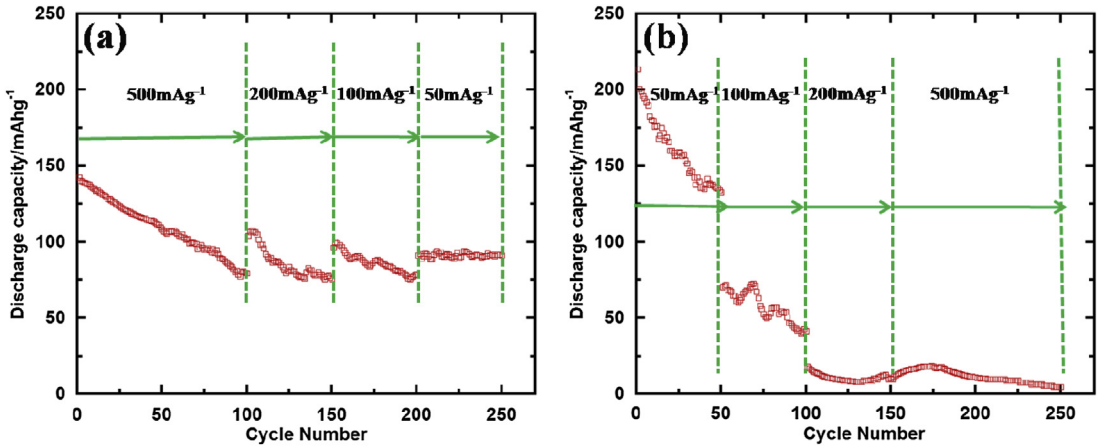

Fig. 6. Cycle performance of VO_2 at different current densities. (a) From 500 mA g^{-1} to 50 mA g^{-1}. (b) From 50 mA g^{-1} to 500 mA g^{-1}.

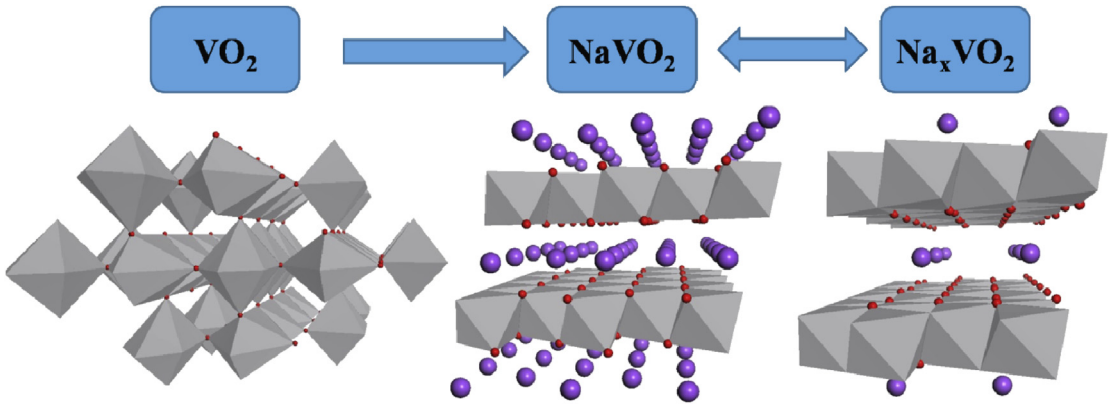

Fig. 7. Scheme of the Na insertion and extraction process.

of Fig. 5(a). At a low current density, the charge and discharge depth is more extensive, and after decades of cycles, fixed interlayer distance and crystallographic structure are formed. Once discharged at a high current density, the original structure is destroyed, and a collapse of the crystallographic structure takes place, leading to a rapid decay of capacity.

The Na ions transmission in charge and discharge process is demonstrated in Fig. 7. Initially, VO_2 nanosheets are synthesized through a hydrothermal method. In the first discharge process, about one Na ion is inserted in a VO_2 molecule, and $NaVO_2$ is formed. Then, in the following charge process, $NaVO_2$ is oxidized to Na_xVO_2 ($x \approx 0.3$). After that, in the discharge process of the second cycle, Na_xVO_2 is once again reduced to $NaVO_2$. The reversible reaction (2) continuously happens as the charge and discharge process goes on.

4. Conclusions

Relying on a simple short-time hydrothermal method, parallel ultrathin nanosheets with an average diameter of ca. 50–60 nm and an average length of hundreds of nanometers were synthesized. First-principles simulations were employed to theoretically investigate the insertion–extraction mechanism of sodium ions in the VO_2 electrode. The VO_2 nanosheets show an excellent performance owing to the following reasons: the high surface-to-volume ratio can increase the contact area with electrolyte; the single-crystalline structure display high crystallinity and provides a mechanically stable structure; the layered structure of Na_xVO_2 can make the intercalation and deintercalation of Na ions much faster and easier.

Combining the formation energy, unit cell volume and lattice parameters changes, and electrochemical tests, the results reveal that the reversible reaction during charge and discharge process can happen between $Na_{0.3}VO_2$ and $NaVO_2$. Excellent electrochemical performance was achieved in this work. This cathode material can work at very high current densities, and even at 1000 mA g^{-1}, the discharge capacity is still maintained at 70 mAh g^{-1} over 50 cycles. If further optimized, it is believed that the VO_2 nanosheets can be used as high-rate cathode material in large-scale energy storage.

Acknowledgments

This work was supported by the National Natural Science Foundation of China (No. 51322402), the Program for New Century Excellent Talents in University (NCET-2011-0577), Ministry of Education of China, the Fundamental Research Funds for the Central Universities (FRF-TP-12-002B), the National Science Foundation of China (No. 11174297) and the National Key Fundamental Research (973) Program of China (No. 2011CB922204).

Appendix A. Supplementary data

Supplementary data related to this article can be found at http://dx.doi.org/10.1016/j.jpowsour.2013.11.016.

References

[1] J.M. Tarascon, N. Recham, M. Armand, J.N. Chotard, P. Barpanda, W. Walker, L. Dupont, Chem. Mater. 22 (2010) 724.
[2] Y. Janssen, D.S. Middlemiss, S.H. Bo, C.P. Grey, P.G. Khalifah, J. Am. Chem. Soc. 134 (2012) 12516.
[3] M. Konarova, I. Taniguchi, J. Power Sources 195 (2010) 3661.
[4] C. Sun, S. Rajasekhara, J.B. Goodenough, F. Zhou, J. Am. Chem. Soc. 133 (2011) 2132.
[5] M. Winter, J.O. Besenhard, M.E. Spahr, P. Novak, Adv. Mater. 10 (1998) 725.
[6] A. Yaksic, J.E. Tilton, Resour. Policy 34 (2009) 185.
[7] F. Risacher, B. Fritz, Aquat. Geochem. 15 (2009) 123.
[8] D.D. MacNeil, J.R. Dahn, J. Electrochem. Soc. 149 (2002) 912.
[9] Y. Cao, L. Xiao, M.L. Sushko, W. Wang, B. Schwenzer, J. Xiao, Z. Nie, L.V. Saraf, Z. Yang, J. Liu, Nano Lett. 12 (2012) 3783.
[10] A. Abouimrane, D. Dambournet, K.W. Chapman, P.J. Chupas, W. Weng, K. Amine, J. Am. Chem. Soc. 134 (2012) 4505.
[11] P. Senguttuvan, G. Rousse, V. Seznec, J.M. Tarascon, M.R. Palacín, Chem. Mater. 23 (2011) 4109.
[12] Y. Cao, L. Xiao, W. Wang, D. Choi, Z. Nie, J. Yu, L.V. Saraf, Z. Yang, J. Liu, Adv. Mater. 23 (2011) 3155.
[13] M. Sathiya, K. Hemalatha, K. Ramesha, J.M. Tarascon, A.S. Prakash, Chem. Mater. 24 (2012) 1846.
[14] F. Sauvage, L. Laffont, J.M. Tarascon, E. Baudrin, Inorg. Chem. 46 (2007) 3289.
[15] P. Moreau, D. Guyomard, J. Gaubicher, F. Boucher, Chem. Mater. 22 (2010) 4126.
[16] K. Trad, D. Carlier, L. Croguennec, A. Wattiaux, M.B. Amara, C. Delmas, Chem. Mater. 22 (2010) 5554.
[17] S. Tepavcevic, H. Xiong, V.R. Stamenkovic, X.B. Zuo, M. Balasubramanian, V.B. Prakapenka, C.S. Johnson, T. Rajh, ACS Nano 6 (2012) 530.
[18] Z.L. Jian, L. Zhao, H.L. Pan, Y.S. Hu, H. Li, W. Chen, L.Q. Chen, Electrochem. Commun. 14 (2012) 86.
[19] H.Y. Wang, W.J. Wang, Y. Ren, K.L. Huang, S.Q. Liu, J. Power Sources 199 (2012) 263.
[20] Y. Yamada, T. Doi, I. Tanaka, S. Okada, J. Yamaki, J. Power Sources 196 (2011) 4837.
[21] R. Alcántara, M. Jaraba, P. Lavela, J.L. Tirado, Chem. Mater. 14 (2002) 2847.
[22] N. Magg, J.B. Giorgi, M.M. Frank, B. Immarapom, T. Schroeder, M. Bäumer, H.J. Freund, J. Am. Chem. Soc. 126 (2004) 3616.
[23] P. Liu, S.H. Lee, H.M. Cheong, C.E. Tracy, J.R. Pitts, R.D. Smith, J. Electrochem. Soc. 149 (2002) 76.
[24] D. Yu, Y. Yang, M. Durstock, J.B. Baek, L. Dai, ACS Nano 4 (2010) 5633.
[25] Y.S. Hu, X. Liu, J.O. Muller, R. Schlogl, J. Maier, D.S. Su, Angew. Chem. Int. Ed. 48 (2009) 210.
[26] C. Nethravathi, B. Viswanath, J. Michael, M. Rajamath, Carbon 50 (2012) 4839.
[27] J. Liu, Q. Li, T. Wang, D. Yu, Y. Li, Angew. Chem. Int. Ed. 43 (2004) 5048.
[28] C.K. Chan, H.L. Peng, R.D. Twesten, K. Jarausch, X.F. Zhang, Y. Cui, Nano Lett. 7 (2007) 490.
[29] C.L. Onnerud, J.O. Thomas, M. Hardgrave, S.Y. Anderson, J. Electrochem. Soc. 142 (1995) 3648.
[30] N.A. Chernova, M. Roppolo, A.C. Dillonb, M. Whittingham, J. Mater. Chem. 19 (2009) 2526.
[31] D.W. Murphy, P.A. Christian, Science 205 (1979) 651.
[32] Q. Zhao, L. Jiao, W. Peng, H. Gao, J. Yang, Q. Wang, H. Du, L. Li, Z. Qi, Y. Si, Y. Wang, H. Yuan, J. Power Sources 199 (2012) 350.
[33] C. Tsang, A. Manthiram, J. Electrochem. Soc. 144 (1997) 520.
[34] M.C. Payne, M.P. Teter, D.C. Allan, T.A. Arias, J.D. Joannopoulos, Rev. Mod. Phys. 64 (1992) 1045.
[35] S.J. Clark, M.D. Segall, C.J. Pickard, P.J. Hasnip, M.J. Probert, K. Refson, M.C. Payne, Z. Kristallogr. 220 (2005) 567.
[36] J.S. Lin, A. Qtseish, M.C. Payne, V. Heine, Phys. Rev. B 47 (1993) 4174.
[37] H.J. Monkhorst, J.D. Pack, Phys. Rev. B 13 (1976) 5188.
[38] T.H. Fischer, J. Almlof, J. Phys. Chem. 96 (1992) 9768.
[39] J.I. Sohn, H.J. Joo, A.E. Porter, C.J. Choi, K. Kim, D.J. Kang, M.E. Welland, Nano Lett. 7 (2007) 6.
[40] F. Sediri, N. Gharbi, Mater. Lett. 63 (2009) 15.
[41] R. Li, C.Y. Liu, Mater. Res. Bull. 45 (2010) 688.
[42] J. Ni, W. Jiang, K. Yu, Y. Gao, Z. Zhu, Electrochim. Acta 56 (2011) 2122.
[43] S. Ji, Y. Zhao, F. Zhang, P. Jin, J. Cryst. Growth 312 (2010) 282.
[44] L. Wang, T. Maxisch, G. Ceder, Phys. Rev. B 73 (2006) 195107.
[45] Y.J. Kang, J.H. Kim, S.W. Lee, Y.K. Sun, Electrochim. Acta 50 (2005) 4784.
[46] F. Nobili, F. Croce, B. Scrosati, R. Marassi, Chem. Mater. 13 (2001) 1642.
[47] L. Su, Y. Jing, Z. Zhou, Nanoscale 3 (2011) 3967.
[48] J. Wang, X. Sun, Energy Environ. Sci. 5 (2012) 5163.
[49] J. Kasperkiewicz, J.A. Kovacich, D. Lichtman, J. Electron Spectrosc. Relat. Phenom. 32 (1983) 128.
[50] N.K. Nag, F.E. Massoth, J. Catal. 124 (1990) 127.
[51] G.S. Zakharova, C. Jähne, A. Popa, C. Täschner, T. Gemming, A. Leonhardt, B. Büchner, R. Klingeler, J. Phys. Chem. C 116 (2012) 8714.
[52] P. Poizot, S. Laruelle, S. Grugeon, L. Dupont, J.M. Tarascon, Nature 407 (2000) 496.
[53] E. Hosono, H. Matsuda, I. Honma, S. Fujihara, M. Ichihara, H.S. Zhou, J. Power Sources 182 (2008) 349.
[54] L.F. Cui, R. Ruffo, C.K. Chan, H.L. Peng, Y. Cui, Nano Lett. 9 (2009) 491.
[55] P. Meduri, C. Pendyala, V. Kumar, G.U. Sumanasekera, M.K. Sunkara, Nano Lett. 9 (2009) 612.
[56] L. Kavan, J. Procházka, T.M. Spitler, M. Kalbác, M. Zukalová, T. Drezen, M. Grätzel, J. Electrochem. Soc. 150 (2003) 1000.